Imaging past the Nyquist Edge using a Novel Stationary Optical Spectrometer

Vinod R. Krishnamoorthy

As a rising freshman, I participated in the Optics Science Olympiad event. The experimental portion of the event particularly interested me. Given several optical devices, I was tasked with designing and executing an experiment that demonstrated a concept such as dispersion or refraction. This experience sparked my interest in optics. I volunteered as an assistant coach for the event in high school, where I gained a deeper understanding of the field through teaching others. This experience made me want to further pursue the field, so I reached out to Professor Y. Fainman, the head of the UC San Diego nano-photonics lab. I was fortunate to be accepted as a volunteer intern starting the summer after my freshman year. I began by just assisting my mentor with data collection, but I gradually grew my understanding until I could contribute to a project on my own. By the end of my sophomore year, I was ready to begin working on the analysis of spectrometers. I applied my mathematics training to analyze how light interference could work with novel geometries derived from Albert Abraham Michelson's classic experiment, and this led to my research paper. I've always loved working with new tools and concepts, and once I understood the relevant background, I was able to make my own contribution.

Throughout high school, I have had a strong affinity for teaching and participating in math competitions. This experience helped me learn the analytical tools to understand scientific principles and equations. I used these techniques to understand concepts such as the Fourier Transform and the complex vector model of electromagnetic waves –which at first were daunting, but understandable and logical in the proper mathematical context, and which ultimately proved very valuable in my research on optical spectroscopy. I used my training numerous times to derive my own formulas and invent algorithms to remove spectral background noise in the data I collected in the lab. I used calculus to lower the error of amplitude calculations, and I predicted the behavior of spatial frequencies past the Nyquist edge with step-by-step mathematical proofs. By mixing mathematics, physics, and engineering, I addressed a wide range of interdisciplinary problems.

Seeing my mathematical models work in the lab was truly exciting and inspiring. The completion of my research project has given me confidence in my ability to work on high-level scientific projects. When I began working at the UCSD lab, I was slightly intimidated because of the difficulty of the material I was trying to understand. Now, I feel confident reading scientific literature, and the comprehension skills and technical language I have learned allow me to read and apply information from any source, college-level textbooks and professional optics journals alike. Before I began this research project, my main academic interest was in competition mathematics – specifically, solving difficult problems that I could tackle in less than an hour. Doing scientific research taught me how rewarding it can be to work at a problem for months before finding the answer. The pride I felt during moments of discovery in my research project were unparalleled in my experiences with math. Not only did completing my project affirm the numerous real-world applications of mathematics, but it also inspired my interest in physics and computer science. The project encouraged me to teach myself Python and to engage in fun side-projects such as writing Python simulators for lenses, mirrors, and standing waves. The research opportunity and the invaluable guidance of my UC San Diego mentors played a major role in my ambitions to pursue a career as a scientific researcher. I gratefully acknowledge my mentor Brandon Hong, Professor Y. Fainman, and the ECE Dept. of UCSD for providing the facilities and opportunity to perform this work.

ABSTRACT

Oftentimes, light that we see is comprised of many different wavelengths. A device called a spectrometer is needed to determine exactly which wavelengths make up the light emitted or absorbed from an everyday light source. Knowing this information has important practical benefits, from determining the identity of specific chemical compounds to analyzing the motion of stars and planets to detecting the presence of harmful gases, and many others. Spectrometers have been widely studied, but every spectrometer has its own strengths and weaknesses. One of the best ways to build a spectrometer is to use an interferometer, a device that analyzes interference patterns to extract information about the light source. Here, I present analysis and a demonstration of stationary interferometry with no moving parts and a camera limited by a finite resolution. I experimentally and analytically show that interference patterns that require much higher resolutions to appropriately display can be distinguished by a combination of their aliased spatial frequency and their contrast. The motivation is to enable higher spatial frequencies to be clearly distinguishable, and hence improve the flexibility and wavenumber resolution (constant finite difference between measurable wavenumbers) of the resulting spectrometer. By moving past numerous Nyquist edges, the wavenumber resolution rapidly improves, allowing for low-cost, stationary, and accurate spectrometers to be constructed. When combined with compact, state-of-the-art semiconductor lasers, the simplicity of the setup and the ability of the system and mathematical algorithm to function with low-resolution cameras (2.3 megapixels) opens the possibility for such compact spectrometers to be eventually implemented on smartphones.

I. INTRODUCTION

The experiment conducted derives and tests the accuracy of formulas for the spatial frequency and modulation transfer function of stationary interferometers. To generate the interference patterns that were to be characterized, different types of stationary interferometers were used[1]. These interferometers split a single beam into two separate beams using a beam splitter, and then send the beams along two separate paths to arrive at the same location. The difference between the lengths of the two paths determines the phase difference between the two beams, and therefore determines the interference pattern that is produced. Slightly rotating a key mirror in each interferometer allows easy manipulation of these path-length differences.

Interference patterns are characterized by the rate at which they alternate between high and low intensities (light and dark), and this property can generally be described by some periodic function. This periodic function equals the sum of a constant (DC) term and sinusoids with different amplitudes. The Modulation Transfer Function characterizes the optical system by determining the spatial resolution of the image as a function of the spatial frequency of the various interference patterns produced by it[2]. The spatial resolution of each image is parameterized by a quantity known as modulation depth, which, assuming a perfectly sinusoidal pattern, equals the amplitude of the sinusoid divided by the average value.

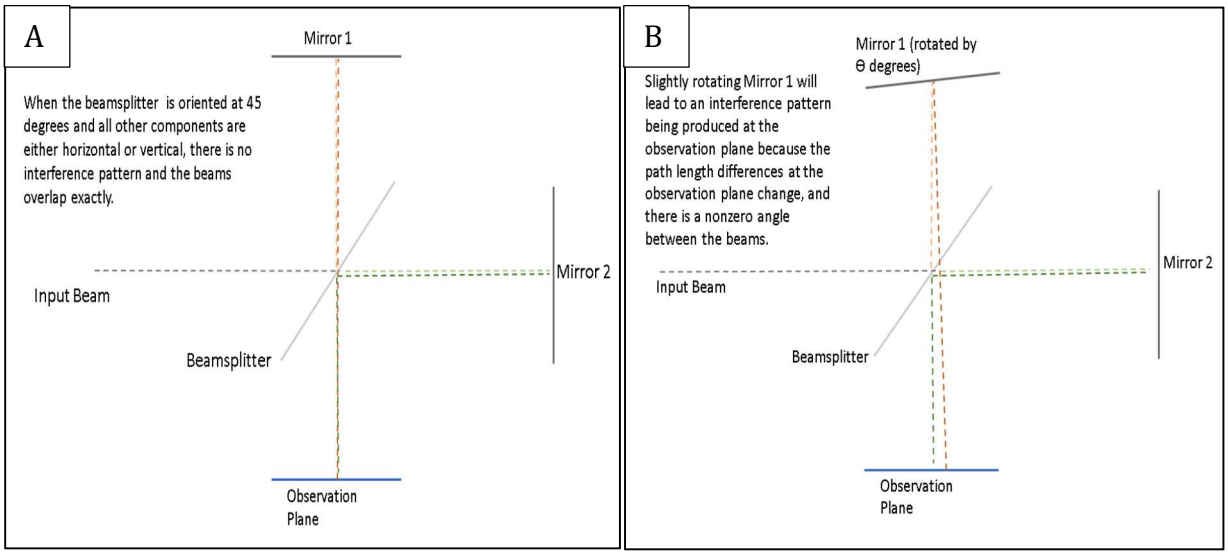

Figure 1: Stationary interferometer based on the Michelson configuration (Interferometer 1): A: No rotation of Mirror 1; B: Small rotation of Mirror 1.

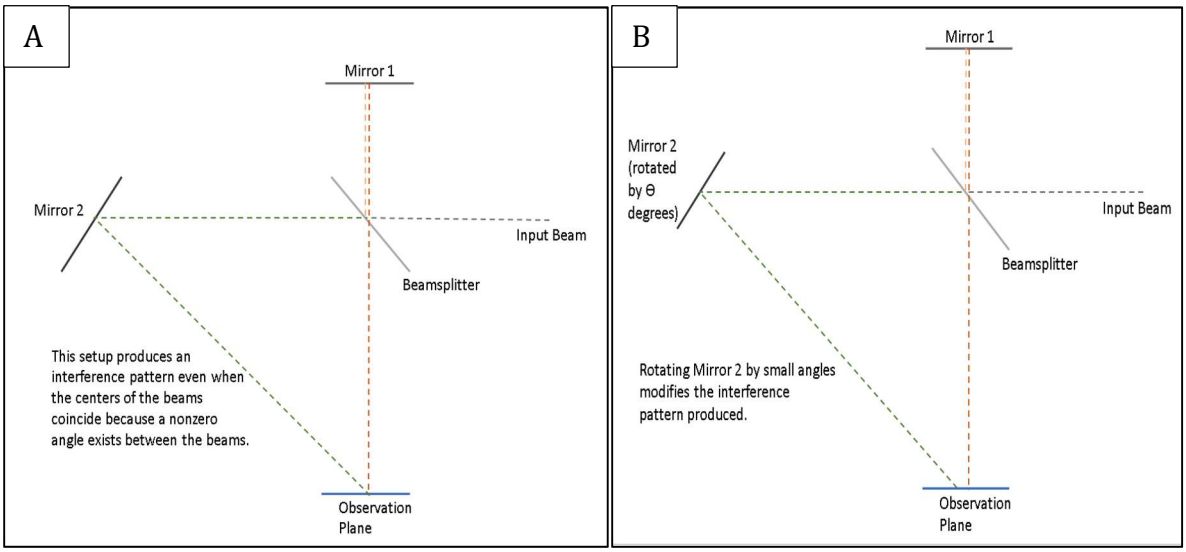

Figure 2: Stationary interferometer based on the modified Michelson configuration (Interferometer 2): A: No rotation of Mirror 2; B: Small rotation of Mirror 2.

II. UNDER-SAMPLING AT DETECTION

Because the detector has only a finite number of samples, a continuous sinusoid cannot be represented in an image of an interference pattern. Any signal with spatial frequency components less than $\frac{1}{2\Delta x}$, where Δx is the width of one sample, has more than enough samples to accurately represent its spatial frequency with the detector. This is an oversampled case. A signal with spatial frequency components greater than $\frac{1}{2\Delta x}$ is under-sampled, which means that it is too high to be accurately represented by the detector. In the case of a camera with a certain number of pixels, the pixels capture the total intensity that reaches them, so the value read by a pixel is the integral of the intensity of the interference pattern within the bounds of the pixel. The under-sampled case can extend the spectral resolution of an interferometer because high interior angles correspond to greater optical path-length differences, which in turn creates a better wavenumber resolution for the interferometric spectrometer. This paper presents and tests a process to utilize the modulation depth of under-sampled spatial frequencies to determine their spatial frequency, even though it is past the Nyquist edge. If higher spatial frequencies are clearly distinguishable, the flexibility and wavenumber resolution of the eventual spectrometer increases.

III. STATIONARY INTERFEROMETER

A stationary mirror interferometer based on the Michelson interferometer was constructed to generate interference patterns with low spatial frequencies, and a modified Michelson interferometer was constructed to generate interference patterns with high spatial frequencies. Figures 1 and 2 show the schematics of these interferometers. Figure 3 shows the actual setup of the Michelson interferometer (Interferometer 1).

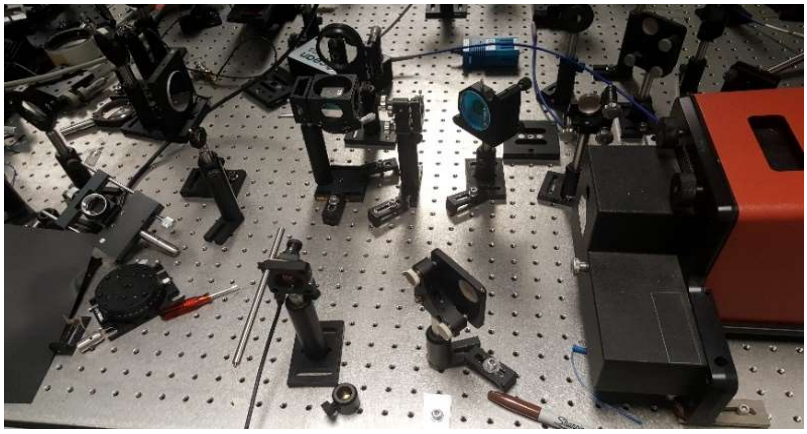

Figure 3: Setup of stationary interferometer based on Michelson configuration (Interferometer 1).

A. SPATIAL FREQUENCY FORMULA

Generally, larger interior angles between the two beams correspond to higher spatial frequencies in the interference pattern. The formula for the intensity of the fringes in one dimension is $I = 4A^2 \cos^2(kx \sin\frac{\alpha}{2} \cos\beta)$, where A is the amplitude of each wave after the initial beam has gone through the beam-splitter, k is the wave number, and $\propto$ is the measure of the angle of divergence between the two beams starting at their intersection point near the observation plane (the beams may have to be extended past the observation plane). β is defined as the measure of the angle between the surface normal to the mirror and the angle bisector of the interior angle between the two beams (the bisector of the angle corresponding to α). This assumes that the amplitude A of the two beams after the beam-splitter is equivalent: if the amplitudes are not equivalent, the interference pattern strays from being a simple sinusoid. For Interferometers 1 and 2, the change in $\propto$ is equivalent to twice the rotation of the chosen mirror about its center. If the rotation of the mirror past its starting point in the counter-clockwise direction is set to be

θ, $2d\theta = d\alpha$. Geometrically, for these interferometers, β is always equal to $\frac{\alpha}{2}$, so the intensity of the interference pattern is $I = 4A^2\cos^2\left(kx\sin\frac{\alpha}{2}\cos\frac{\alpha}{2}\right) = 4A^2\cos^2\left(\frac{kx\sin\alpha}{2}\right) = 2A^2 + 2A^2\cos(kx\sin\alpha)$. The true spatial frequency of an interference pattern with interior angle α is therefore $\frac{k\sin\alpha}{2\pi}$.

B. CAMERA EFFECTS AND MODLUATION TRANSFER FUNCTION

In the experiments, sets of images were created by rotating the mirror by different amounts, starting from the point of full overlap of the beams. The camera used was a 2-D grayscale camera (Point Grey Blackfly USB 23S6M-C mono), with a resolution of 1200x1920 and a pixel width of 5.86 micrometers. The coherent light source used throughout the experiment was a 630 nm red laser. 1200x1920 pixels corresponds to a resolution of 2.3MP, which is less than most modern cell phone cameras.

It was previously shown that the intensity *I* of an interference pattern generated by one of the interferometers is $I = 2A^2 + 2A^2\cos(kx\sin\alpha)$. It is assumed that the original 2D interference pattern is perfectly vertical and is collapsed into one dimension by taking the average of each column. Letting $Q = k\sin\alpha$, to calculate the intensity value of one pixel, the camera effectively performs the integral $\int_{n(\Delta x)}^{(n+1)(\Delta x)}(2A^2 + 2A^2\cos(Qx))dx = 2\Delta xA^2 + \frac{2A^2}{Q}\sin\frac{Q\Delta x}{2}\cos(Q\Delta xn + \frac{Q\Delta x}{2})$, where *n* is the pixel number and Δx is the pixel width. It follows that the coefficient of the DC average should be $2\Delta xA^2$, and the AC coefficient should be $\left|\frac{2A^2}{Q}\sin\frac{Q\Delta x}{2}\right|$. Because of the effects of the exposure of the camera and the intensity of the laser on the amplitude of the interference pattern, it would be difficult to calculate the theoretical value of the amplitude A, making it difficult to calculate either the theoretical AC coefficient or the theoretical DC coefficient independently. However, the ratio of the theoretical AC coefficient to the theoretical DC coefficient is $\left|\frac{\sin\frac{Q\Delta x}{2}}{Q\Delta x}\right|$, which is completely independent of A, so this ratio is what will be measured. Based on the formula, an interference pattern's spatial frequency in inverse meters is $\frac{k\sin\alpha}{2\pi}$, and therefore, the

modulation transfer function relating the interference pattern's true spatial frequency in inverse meters f and the AC/DC ratio (modulation depth) is $\text{modulation depth} = \frac{1}{2}\left|\frac{\sin(\pi f \Delta x)}{\pi f \Delta x}\right|$.

C. NYQUIST EDGE TRAVERSAL

With a set of 1D interference patterns with linearly increasing spatial frequencies, the spatial frequencies measured by FFT analysis of the sampled interference patterns linearly increase as well until the first Nyquist edge. A simple cosine wave in the space domain with a spatial frequency exactly at the first Nyquist edge would be $\cos(\pi n)$, where $n \in \mathbb{Z}$ and represents the pixel number. The angular frequency π would be in units of radians per sample. A positive increase in angular frequency Δf would force the true spatial frequency to be unrepresentable because it would be past the first Nyquist edge. Comparing the true signal $\cos(\,(\pi + \Delta f)n\,) = \cos(\pi n + n\Delta f) = \cos(\pi n)\cos(n\Delta f) - \sin(\pi n)\sin(n\Delta f)$ and the representable signal $\cos(\,(\pi - \Delta f)n\,) = \cos(\pi n - n\Delta f) = \cos(\pi n)\cos(n\Delta f) + \sin(\pi n)\sin(n\Delta f)$, it is clear that they are always equivalent, because n is always an integer and $\sin(\pi n)$ is always equal to zero. This equation predicts that a sinusoid with a spatial frequency past the Nyquist edge will look like a sinusoid with a spatial frequency below the Nyquist edge when it is sampled, and as the true spatial frequencies of an interference pattern increase past the Nyquist edge, the aliased spatial frequencies will bounce off the Nyquist edge and decrease at the rate that the true spatial frequencies increase. The aliased spatial frequency will later bounce off the zero-frequency point and subsequent Nyquist edges and zero-frequency points as well. A formula for the aliased spatial frequency of a signal with true spatial frequency f in inverse samples is $0.5 - |0.5 - (f \bmod 1)|$. Substituting in $f = \frac{k \sin\alpha}{2\pi}$, the aliased spatial frequency becomes $\frac{1}{2\Delta x} - \left|\frac{1}{2\Delta x} - (\frac{k \sin\alpha}{2\pi} \bmod \frac{1}{\Delta x})\right|$ in inverse meters. A true spatial frequency f in inverse samples is $\lfloor 2f \rfloor$ Nyquist edges past an oversampled spatial frequency, where $\lfloor x \rfloor$ is the greatest integer less than or equal to x. If given a sampled spatial frequency $\dot{f}$ in inverse meters, the true spatial frequency f in inverse meters can be $f = \frac{N}{\Delta x} - \dot{f}$ or $f = \frac{N}{\Delta x} + \dot{f}$, where Δx is the width of one pixel and N is any integer.

The setup for Interferometer 1 is easily oversampled. The interior angle between the beams only slightly diverges from zero degrees before the beams no longer overlap, so for a camera with a moderately large resolution, a Nyquist edge is not reached. In the type of setup described by Interferometer 2, under-sampling is much more likely because the interior angle is much higher. For the setup of Interferometer 2 used in this experiment, the initial interior angle is $\propto \approx 26.2\,°$. By the formula $I = 2A^2 + 2A^2\cos(kx\sin\alpha)$, the spatial frequencies should be close to $3.48 * 10^5$ inverse meters, based on the initial interior angle. Because the pixel width is $5.86 * 10^{-6}$ meters, this spatial frequency is $\lfloor 2\Delta xf \rfloor = \left\lfloor 2 * (3.48 * 10^5) * (5.86 * 10^{-6}) \right\rfloor = 4$ Nyquist edges past an oversampled spatial frequency. The Nyquist edge seen to be traversed in the data set is therefore the 4th Nyquist edge.

IV. DESCRIPTION OF EXPERIMENT

The objective of this experiment is to confirm the accuracy of the formula for modulation depth as a function of the spatial frequency of an interference pattern generated by a stationary interferometer. With a reasonably high accuracy in both the over-sampled and under-sampled cases, a stationary interferometer can measure interference patterns with spatial frequencies well past the first Nyquist edge. A stationary interferometer functioning as a spectrometer will be able to use the modulation depth, measured spatial frequency, and interior angle between the beams to find the wavenumber k through simple inverse operations. Although the interior angle varied with the rotation of a corner mirror in this experiment, in a true stationary spectrometer, all the mirrors will be fixed in place, and the interior angle between the two beams will be fixed at some angle. The ability for the stationary interferometer to function at high interior angles vastly improves the wavenumber resolution (Δk, the difference between measurable wavenumbers) of the eventual spectrometer.

A. PROCEDURE

The images were formed by linearly increasing the rotation of the mirror and capturing the interference patterns formed with a camera. The purpose of scanning through different amounts rotation

of the mirror was to gain a wider breadth of interior angles to analyze. The wavelength of the laser used in the interferometer was 630 nm, so the wavenumber $k = \frac{2\pi}{630*10^{-9}} = 9{,}973{,}310$ radians/meter.

The analysis presented uses the aliased spatial frequency combined with rough setup measurements to calculate the theoretical spatial frequency and AC/DC ratio, and then compares this theoretical ratio with the measured AC/DC ratio. The measurements of the setup are used to determine the number of Nyquist edges past an oversampled spatial frequency the interference pattern is at, which is necessary for conversion from the aliased spatial frequency to the actual spatial frequency.

B. IMAGE-PROCESSING USING RADON TRANSFORM

A raw interference pattern from a camera has two inherent issues which make it difficult for computer algorithms to detect the proper spatial frequency and modulation depth. The first issue is that the orientations of the beams and the camera may not line up along the same plane. This will cause the fringes to appear at an angle with respect to the camera frame, and this angle will be constantly changing as the beams overlap by different amounts. The second issue is that the amplitude of the sampled sinusoid cannot be accurately determined by simply taking the Fourier Transform because the sinusoids become truncated, and there are not enough data points to find the true amplitude. To combat the rotation issue, the Radon Transform along with additional processing was used to straighten the interference pattern. The Radon Transform for a single angle essentially rotates the image by that angle and vertically sums the image after rotation, creating a row vector. The Radon Transform for a set of angles does this once per angle and puts the results together into a 2-D image called a sinogram. The row vector with the highest modulation depth (AC peak/DC peak) corresponded to the angle at which the fringes were the straightest. The Radon transform over the set of angles {-20, -19.9, -19. 8…19.8,19.9,20.0} (degrees) was applied to each image. After the ideal angle was found, the image was rotated by that angle. After rotation, the image had to be cropped to ensure that the window of the image would be oriented parallel to the axes. Since the resulting image of the interference pattern was almost exactly vertical, the mean of each column was taken to collapse the 2D image into one row vector. To combat the truncation issue, the amplitude was calculated as the

maximum of the resulting row vector minus the minimum of the row vector instead of the normalized peak height in the frequency space. This ensured that the effects of truncated sinusoids were minimized because the maximum and minimum of a perfect sinusoid are inherently the least truncated cycles in the waveform. However, this created greater subjectivity to noise, because there was less space for noise to average out.

The algorithm was tested with a training set of computer-generated fringes. The training set had a noise coefficient that was approximately 11.8% of the average intensity, a background signal with an amplitude of approximately 9.4% of the average intensity, and a true signal with an amplitude of approximately 23.5% of the average intensity. A set of 12 images was created by rotating the fringes using rotation matrices on the coordinates. The standard deviation of the modulation depths was approximately 0.70 percent of the mean, and the standard deviation of the spatial frequencies was near-zero at 2.16e-14 percent of the mean. From this result, it can be determined that the algorithm is effective at eliminating the angle of the fringes and noise as confounding variables in determining modulation depth and spatial frequency for signals of sufficient strength.

V. RESULTS

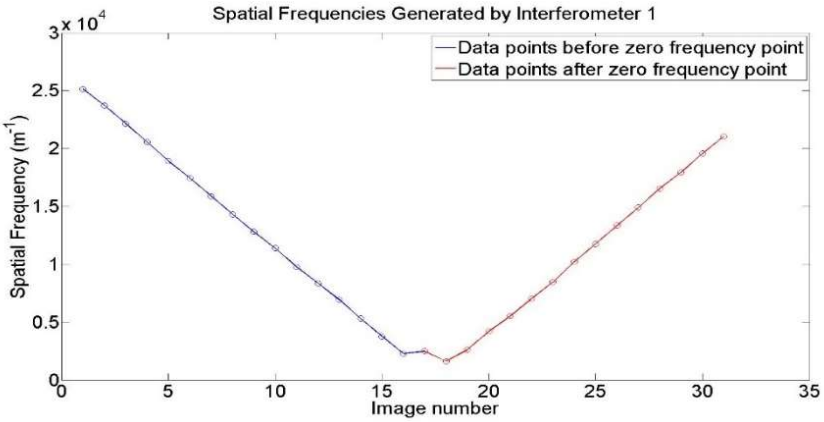

Figure 4: Spatial frequencies of 31 images generated by the experiment with Interferometer 1.

For Interferometer 1, the generated spatial frequencies ranged from 1,622 to 25,133 inverse meters. These frequencies were oversampled, and this spatial frequency range corresponds to an angle range of 0.029 to 0.454 degrees. Figure 5 relates the measured spatial frequency to the modulation depth (AC

coefficient divided by the DC coefficient). The theoretical function was $\frac{1}{2}\left|\frac{\sin(\pi f \Delta x)}{\pi f \Delta x}\right|$. Here, since the signal is oversampled, $\dot{f} = f$, where $\dot{f}$ is the measured spatial frequency and f is the true spatial frequency. The measured spatial frequencies are shown in Figure 4. The measured Modulation Transfer function is shown in Figure 5. The average error, not including the two outlier points with spatial frequencies that were not detectable because their rotation angles were out of range for the Radon Transform, was 7.22%.

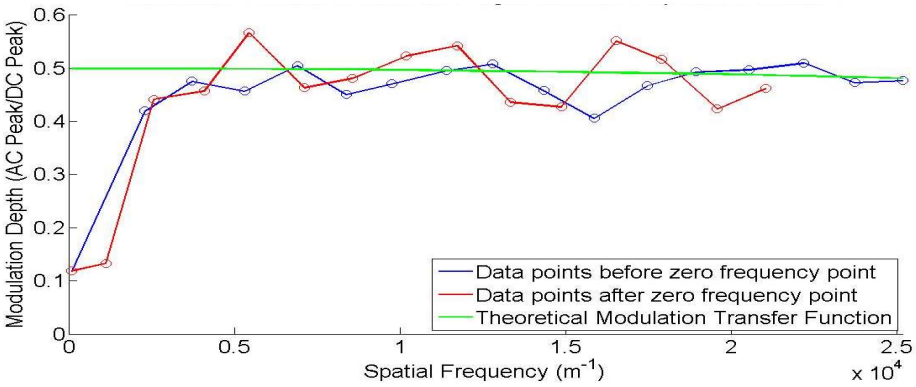

Figure 5: Modulation Transfer Function for the 31 images generated by Interferometer 1.

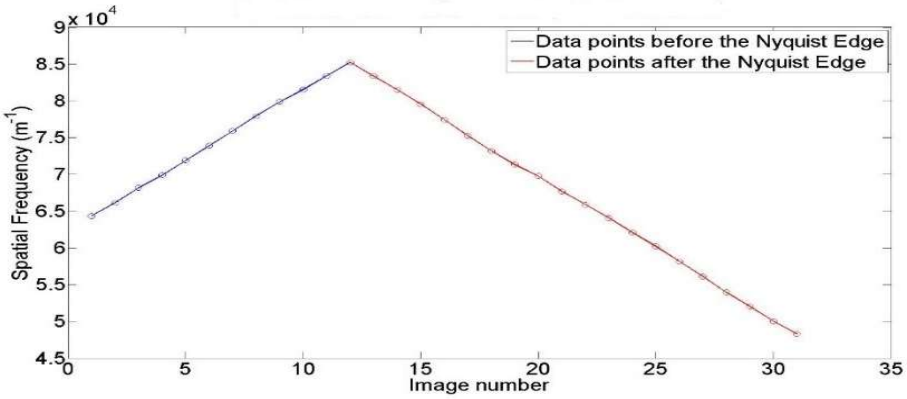

Figure 6: Spatial frequencies of 31 images generated by the experiment with Interferometer 2.

For Interferometer 2, the measured spatial frequencies generated ranged between 48,300 and 85,213 inverse meters. This is a traversal of the fourth Nyquist edge, so the true spatial frequencies before the Nyquist edge are $f = \frac{3}{\Delta x} + \dot{f}$, where $\dot{f}$ is the measured spatial frequency in inverse meters and Δx is the pixel width, and the true spatial frequencies after the Nyquist edge are $f = \frac{4}{\Delta x} - \dot{f}$. The range of true spatial frequencies is 447,570 to 730,890 inverse meters. This corresponds to an interior angle range of 16.4 to

27.4 degrees. The measured spatial frequencies are shown in Figure 6. The measured Modulation Transfer Function is shown in Figure 7. The average error from the theoretical modulation transfer function was 20.3 percent, where all thirty-one data points were included.

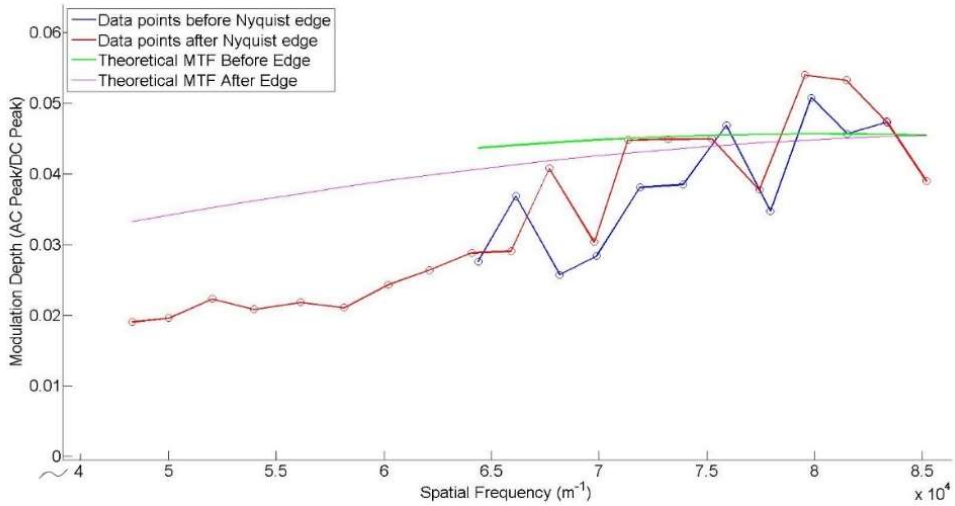

Figure 7: Zoomed in plot of the Modulation Transfer Function for the 31 images generated with Interferometer 2.

VI. DISCUSSION AND CONCLUSIONS

This paper discussed work towards making stationary interferometers capable of analyzing interference patterns well past the traditional Nyquist edge limits of cameras with resolutions comparable to those commonly available in smartphones. The experiment conducted derives and tests the accuracy of formulas for the spatial frequency and modulation transfer function of stationary interferometers given rough measurements of their setup.

Based on the results, it can be concluded that a spectrometer based on a stationary interferometer can be constructed with a high interior angle that produces interference patterns many Nyquist edges past an oversampled spatial frequency. There was a reasonable degree of error in the experiment (7.22% for the over-sampled case and 20.3% for the under-sampled case), but the principle that such a spectrometer can be constructed is still validated by the data.

Fortunately, some degree of error in the measured modulation depth is tolerable by the system if the spatial frequency measurement is accurate. For any measured spatial frequency $\dot{f}$, the potential true spatial frequencies are $\frac{N}{\Delta x} - \dot{f}$ and $\frac{N}{\Delta x} + \dot{f}$, where Δx is the pixel width and N is any integer. A spectrometer would only have to use the modulation depths to distinguish these potential spatial frequencies from each other. Unfortunately, this task becomes more difficult as the true spatial frequencies become higher because the corresponding modulation depths are closer to each other, but only when the spatial frequencies become higher does the wavenumber resolution of the spectrometer increase. An illustration of this idea for an example value of $\dot{f}$ is shown below.

Potential Spatial Frequency (m^{-1})	Theoretical Modulation Depth
65,000	0.389
105,648	0.239
235,648	0.107
276,297	0.091
406,297	0.062
446,945	0.057
576,945	0.044
617,594	0.041

Table 1: Potential Spatial Frequencies for a Measured Spatial Frequency of 65,000 m^{-1}

The error for the stationary interferometer based on the Michelson interferometer (Interferometer 1) is well within the allowable range. However, Figure 7 shows that the modified Michelson interferometer used in this experiment, which was oriented so that the beams would have an interior angle of about 26 degrees, has too high an error to be an accurate spectrometer at this stage. In this experiment, the idea of a spectrometer with improved resolution based on this stationary interferometer was validated, but the error needs to be reduced for this to be a reality.

Future experimentation will use similar stationary interferometers to construct real spectrometers at a fixed angle. Knowing the accuracy of the formula for sampled spatial frequency $\frac{1}{2\Delta x} - \left|\frac{1}{2\Delta x} - (\frac{k \sin \alpha}{2\pi} \bmod \frac{1}{\Delta x})\right|$ and the modulation transfer function $\frac{1}{2}\left|\frac{\sin(\pi f \Delta x)}{\pi f \Delta x}\right|$, k can be calculated from the measured data if the interior angle between the beams (α) is known. High resolution for k will be achieved if the

angle α is high because the resolution for both interferometers is $\Delta k = \frac{1}{2X_o \sin\alpha \cos\frac{\alpha}{2}}$ where X_o is the width of the camera, α is the interior angle, and $\frac{\alpha}{2}$ is the bisector angle. In this case, $X_o = 0.0112512$ m. For Interferometer 1, with interior angles close to 0 degrees, for example, 0.454 degrees, the wavenumber resolution would be $\Delta k = \frac{1}{2X_o \sin 0.454° \cos .227°} \approx 5610$ inverse meters, while the wavenumber resolution of an interferometer with a 26 degree interior angle would be $\Delta k = \frac{1}{2X_o \sin 26° \cos 13°} \approx 104$ inverse meters, over fifty times smaller. However, the increase in resolution would come at a loss in modulation depth (a.k.a. contrast), which makes the signal more subject to noise.

Since wavenumber resolution is somewhat obscure, I will relate it to wavelength resolution. Wavelength resolution is not constant with respect to wavelength, so a local wavelength λ_0 will be introduced at which the resolution $\Delta\lambda$ will be calculated. By the definition of wavenumber, $\Delta k = \left|\frac{2\pi}{\lambda_0+\Delta\lambda} - \frac{2\pi}{\lambda_0}\right|$. Rearranging, $\Delta\lambda = \frac{\Delta k(\lambda_0)^2}{(\Delta k)(\lambda_0)+2\pi}$. With a wavenumber resolution of 5610 inverse meters, the wavelength resolution for a 630 nm source would be 0.354 nanometers, but with a wavenumber resolution of 104 inverse meters, the wavelength resolution would be 0.00657 nanometers.

Despite its limitations, a stationary interferometer that detects beyond the Nyquist edge and can function as a spectrometer has been constructed. The ability to detect past the Nyquist edge greatly increases its resolution. Setups like this one can be implemented on smartphones, potentially provided mass access to cheap spectrometry. This type of stationary spectrometer is ideal for this purpose because it contain no moving parts unlike other "scanning" spectrometers[1], and the components (mirrors, beam-splitters, camera) are either cheap to add on or already present on a smartphone. The setup is also very simple compared to other common spectrometers, which makes it easy to shrink the system down. This technology can also be used to determine the identities of chemical compounds through Fourier-Transform Infrared spectroscopy (FTIR) analysis[3-6].

This paper has presented a pathway to a compact interferometer that could eventually be used in a spectrometer with a low-cost camera. A key component of such a spectrometer, particularly one that could

be used for chemical compound and harmful gas detection, is a mid-wave to long-wave laser source. Over the last two decades, we have seen breakthrough research at Bell Labs[7], Harvard University[8], and Princeton University[9] and other leading research institutions towards the development of quantum-cascade lasers operating at mid-IR wavelengths. This technology has recently been commercialized to produce lasers only a few mm in size over the whole mid-wave and long-wave infrared spectral regions[10], thereby making a compact laser source for the stationary spectrometer described in this paper a reality.

VII. REFERENCES

1. M.-L. Junttila, J. Kauppinen, and E. Ikonen, "Performance limits of stationary Fourier spectrometers," *J. Opt. Soc. Am. A* vol. 8, pp. 1457-1462, 1991.
2. G. D. Boreman, Modulation Transfer Function in Optical and Electro-Optical Systems, SPIE Press, Bellingham, WA (2001).
3. L. Rodriguez-Saona, M. Allendorf, "Use of FTIR for rapid authentication and detection of adulteration of food," *Annu. Rev. Food Sci. Technol.* vol. 2, pp. 467–483, 2011.
4. L. M. Freeman, A. Smolyaninov, L. Pang, Y. Fainman, "Simulated Raman correlation spectroscopy for quantifying nucleic acid-silver composites," *Sci. Rep.* vol. 6, pp. 1-8, 2016.
5. P. R. Griffiths, J. A. De Haseth, Fourier transform infrared spectrometry, vol. 171, John Wiley & Sons, (2007).
6. J. R. Ferraro, L. J. Basile, Fourier transform infrared spectra: applications to chemical systems, Academic Press, (2012).
7. F. Capasso, C. Gmachl, D. L. Sivco, and A. Y. Cho "Quantum cascade lasers," *Physics Today* vol. 55, pp. 34-38, 2002.
8. Pflugl C, Diehl L, Tsekoun A, Go R, Patel CKN, Wang X, Fan J, Tanbun-Ek I, Capasso F, "Room-temperature continuous-wave operation of long wavelength (lambda=9.5μm) MOVPE-grown quantum cascade lasers," *Electron. Lett.* vol. 43, pp. 1026-1028, 2007.
9. Liu PQ, Hoffman AJ, Escarra MD, Franz KJ, Khurgin JB, Dikmelik Y, Wang X, Fan JY, Gmachl C, "Highly power-efficient quantum cascade lasers," *Nature Photonics* vol. 4, pp. 95 - 98, 2010.
10. Laser Specifications, 2009. Retrieved from http://atoptics.com/laser_specs.html.

VIII. APPENDIX A: ALGORITHM DESIGN

Task: Find the spatial frequency and modulation depth of a 2D interference pattern

Input: MATLAB cell array of the 2D interference patterns taken by the camera

Output: Row vectors with the spatial frequencies, AC coefficient values, and DC coefficient values

1. Initialize the row vectors to store the spatial frequencies, AC coefficient values, and DC coefficient values. Also, create a row vector with the angles to be used in the Radon Transform – projections will only be taken at these angles.
2. For loop traversing through the images in the image cell
    a. Subtract the prerecorded background from the image to get the pure fringe pattern
    b. Find the Radon Transform of the region of the image containing fringes.
    c. Display the 2-D sinogram (result of the Radon Transform) as a scaled image. Prompt the user to input one column with visible contrast. This step is shown in Figure 8.
    d. Plot the FFT (Fast Fourier Transform) of the data in that column and display the plot along with a draggable and scalable rectangle object on the plot.
    e. Prompt the user to drag and scale the rectangle so that the horizontal width of the rectangle spans the AC peak. The maximum y-value over the x-region spanned by the rectangle should be the AC peak height. This step is shown in Figure 8.
    f. Prompt the user to drag and scale another draggable and scalable rectangle object so that the horizontal width of the rectangle spans the DC peak. The maximum y-value over the x-region spanned by the rectangle should be the DC peak. This step is shown in Figure 8.
    g. For loop traversing through each column of the sinogram
        i. Take the column of the sinogram and convert it into a row vector
        ii. Calculate the modulation depth of each column.
        iii. Find the column of the sinogram with the highest modulation depth (highest contrast).
    h. Rotate the image by the angle found so that the image is completely straight.
    i. Collapse this 2D image into a 1D row vector by taking the mean of each column.
    j. Find the spatial frequency, AC, and DC peaks using the FFT of the row vector.
    k. Apply a lowpass filter to the row-vector
    l. Subtract the filtered row-vector from the original row-vector
    m. Find the amplitude of this row-vector by subtracting the minimum of the row-vector from the maximum of the row-vector and dividing by 2

n. Find the amplitude of the filtered row-vector by subtracting the minimum of the row-vector from the maximum of the row-vector and dividing by 2

o. Calculate modulation depth

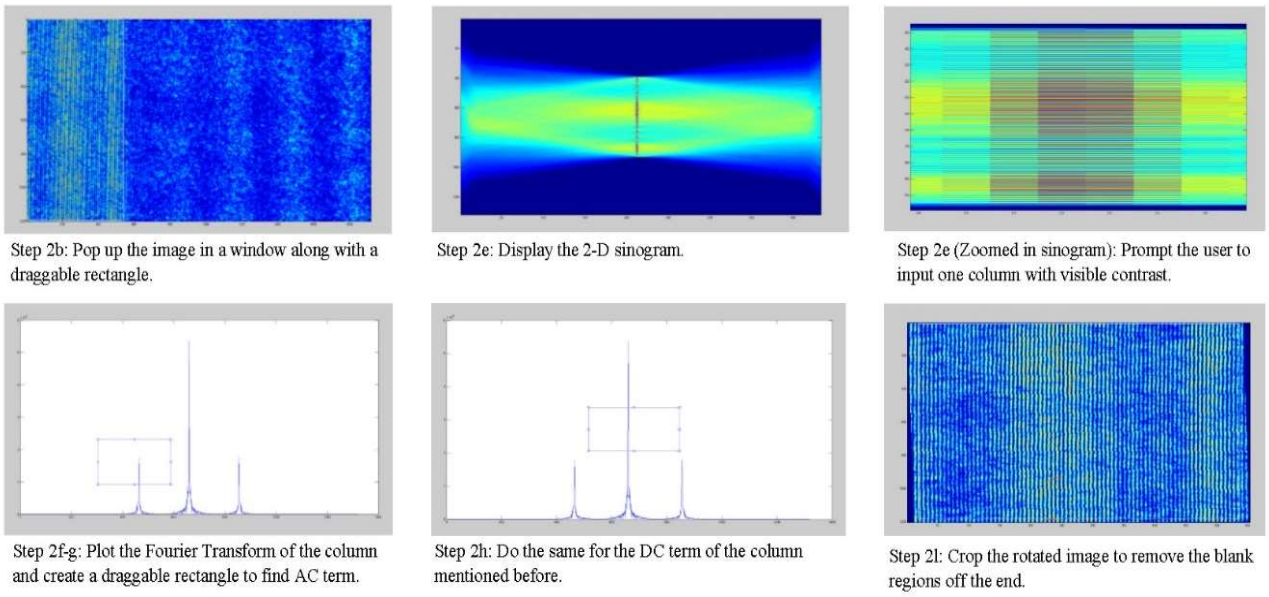

Figure 8: Visual user input portions of the algorithm (clockwise from top left): Step 2b – user selects region with fringes; Step 2e – Radon transform result is displayed; Step 2e (zoomed in sinogram) – centered and expanded Radon transform result; Step 2f-g – user selects AC coefficient from FFT of fringe pattern; Step 2h – user selects DC coefficient from FFT of fringe pattern; Step 2l – user removes slanted edges from rotated result.